RSC Advances

ROYAL SOCIETY OF CHEMISTRY

www.rsc.org/advances

Journal Name

RSCPublishing

ARTICLE

Facile synthesis of Co_3O_4 porous nanosheets/reduced graphene oxide composites and their excellent supercapacitor performance

Cite this: DOI: 10.1039/x0xx00000x

Received 00th January 2012,
Accepted 00th January 2012

DOI: 10.1039/x0xx00000x

www.rsc.org/

Lianbo Ma,[a] Hu Zhou,[b,c] Xiaoping Shen,*[a] Quanrun Chen, [a] Guoxing Zhu [a] and Zhenyuan Ji [a]

Co_3O_4/RGO composites with Co_3O_4 porous nanosheets attached on reduced graphene oxide (RGO) sheet were fabricated through a facile refluxing method followed by a thermal annealing process. Pores with sizes of several nanometers are uniformly distributed in Co_3O_4 nanosheets. The composites as electrode materials for supercapacitors were investigated. They deliver a specific capacitance as high as 518.8 F g^{-1} at the current density of 0.5 A g^{-1}, and great cycling stability with a decay of about 7.6% after 1500 continuous charge-discharge cycles at the current density of 10 A g^{-1}. The excellent capacitive performance can be attributed to the excellent electrical properties, large surface area and well-connected conductive network derived from the structural advantages of the Co_3O_4 porous nanosheets and RGO support. The facile synthesis and the excellent capacitive performance make the Co_3O_4/RGO composites a promising candidate for electrode materials in electrochemical energy storage systems.

Introduction

Supercapacitors have became attractive power sources as energy storage devices due to their outstanding properties such as high power density, long cycle life, fast charging/discharging process and small environmental impact.[1,2] Currently, there are three major types of electrode materials for supercapacitors: metal oxides/hydroxides, carbon materials and conducting polymers.[3-5] Among them, metal oxides with variable valence have been widely investigated as candidates for supercapacitor electrodes in view of their multiple oxidation states for pseudocapacitance generation.[6] However, due to the intrinsic poor electrical conductivity of metal oxides and short diffusion distance of electrolytes into pseudocapacitor electrodes, only the surface part of active materials can effectively contribute to the capacitance. While the underneath parts could hardly participate in the electrochemical charge storage process,[7-9] which often cause poor capacitive performance and seriously hinder the practical application of metal oxides materials. Thus, great efforts have been devoted to avoid these limitations of metal oxides. Up to now, three feasible methods are usually adopted: (i) designing and fabricating hierarchical structure,[10,11] (ii) synthesizing materials directly on current collectors,[12] (iii) preparing carbon-based composites.[13,14]

In recent researches, carbonaceous materials are generally adopted to enhance the capacitive performance of metal oxides.[15,16] Especially, graphene, a newly invented carbon material, is endowed with many favorable properties such as excellent electron transport, large surface area, good mechanical flexibility and strong thermal/chemical stability.[17,18] The incorporation of graphene sheets into the oxides can potentially construct conductivity network and effectively buffer the volume change effect. For instances, nanostructured graphene-based composites such as MnO_2/RGO (RGO = reduced graphene oxide),[19] SnO_2/RGO,[20] RuO_2/RGO,[21] CeO_2/RGO,[22] MoO_3/RGO[23] and Cu_2O/RGO[24] have been applied as electrode materials for supercapacitors, which exhibit much better electrochemical performance in comparison with their bare counterparts.

As a typical transition metal oxide, Co_3O_4 is one of the most investigated electrode materials because of its highly electroactive nature and ultrahigh theoretical specific capacitance value (3560 F g^{-1}).[25-27] Several Co_3O_4/RGO composites with different microstructures have recently been reported.[28-32] For examples, Guan *et al.* prepared a Co_3O_4/RGO composite with needle-like Co_3O_4 anchored on RGO sheets *via* a hydrothermal method.[31] Park *et al.* synthesized Co_3O_4 nanoparticles on RGO sheets through ultrasonication and microwave-assisted method.[32] Despite the enhanced specific capacitances of these Co_3O_4/RGO composites compared to the corresponding pure Co_3O_4, the specific capacitance values of

these composites are still low (usually smaller than 350 F g^{-1}). This may be mainly influenced by the penetration of the electrolytes and surface Faradaic reaction, which generally depend on the morphology, porosity and crystallinity of the nanostructured electrodes.[33] Recently, it was demonstrated that nanosheets with porous structure are favorable to efficient ion and electron transport, and can better accommodate the structure change during charge/discharge processes.[34,35] Inspired by this discovery, we have recently devoted ourselves to the composite electrode materials based on porous metal oxide nanosheets and graphene. In this paper, we report the fabrication of porous Co_3O_4 nanosheets/RGO composites and demonstrate the excellent capacitive performance of the porous nanosheets-based RGO composites.

Experimental

Materials

Natural flake graphite with a particle size of 150 μm (99.9% purity) was purchased from Qingdao Guyu Graphite Co., Ltd. All of the other chemical reagents used in our experiments are of analytical grade, purchased from Sinopharm Chemical Reagent Co., Ltd, and used without further purification. Graphite oxide was prepared from natural flake graphite using a modified Hummers method.[36]

Synthesis of Co_3O_4/RGO composites

In a typical synthesis, 50 mg of the obtained graphite oxide was dispersed into 75 ml deionized water through ultrasonication to form a homogeneous graphene oxide (GO) suspension. Subsequently, certain amount of $Co(NO_3)_2$ $6H_2O$ was added into the above solution gradually under vigorous stirring. After stirring for about 1 h, 10 mmol of hexamethylenetetramine (HMTA) was introduced into the above solution, and then the resultant solution was kept stirring for 1 h. After that, the mixture was refluxed at 90 ℃ for 3 h. After the solution was cooled down to room temperature naturally, the sediments were collected through centrifugation, washed with deionized water and absolute ethanol for several times, and dried in a vacuum oven at 45 ℃ for 24 h. The as-obtained samples were then annealed at 300 ℃ in air for 2 h in order to achieve the final products. The products were designated as Co_3O_4/RGO-0.25, Co_3O_4/RGO-0.50, Co_3O_4/RGO-0.75 and Co_3O_4/RGO-1.0 for the feeding amount of 0.25, 0.50, 0.75 and 1.0 mmol of $Co(NO_3)_2$ $6H_2O$, respectively. For comparison, pure Co_3O_4 nanosheets and bare RGO were prepared in the same way as Co_3O_4/RGO-0.50 composite in the absence of graphite oxide and $Co(NO_3)_2$ $6H_2O$, respectively.

Instrumentation and measurements

The morphology and size of the as-prepared products were examined by scanning electron microscopy (SEM, JSM-6480) and transmission electron microscopy (TEM, JEM-2100). The phase structures were characterized using X-ray diffraction (XRD, Bruker D8 ADVANCE) with Cu-Kα radiation (λ = 1.5406 Å) at a scanning rate of 7° min^{-1}. The composition of the products was determined by energy-dispersive X-ray spectrometry (EDS) and inductively coupled plasma optical emission spectrometry (ICP-OES, Vista-MPX). EDS was recorded with an energy dispersive spectrometer attached to the scanning electron microscope (JSM-6480). Raman scattering was performed on a DXR Raman spectrometer using a 532 nm laser source. Fourier transform infrared (FT-IR) spectra were recorded on a Nicolet Nexus 470 spectrometer with KBr pellets. The Brunauer-Emmett-Teller (BET) surface areas of the products were tested using a surface area and porosity analyzer (NDVA-2000e).

Electrochemical measurements

Electrochemical measurements were carried out on a typical three-electrode system using a CHI 760D electrochemical analyzer (Chen Hua Instruments, Shanghai, China) at room temperature. Pt foil and Hg/Hg_2Cl_2 (Saturated KCl) were used as the counter and reference electrode, respectively. The working electrodes were prepared by mixing 80 wt% active materials (Co_3O_4/RGO composites, Co_3O_4 or RGO), 10 wt% acetylene black and 10 wt% poly(vinylidene fluoride) (PVDF) binder in N-methyl-2-pyrrolidone solvent to form a homogeneous slurry. The slurry was then pasted onto a nickel foam (1×1 cm^2). After that, the nickel foam was placed into a vacuum oven at 60 ℃ to remove the solvent. Cyclic voltammery (CV), chronopotentiometry and electrochemical impedance spectroscopy (EIS) techniques were performed to evaluate the electrochemical properties of the as-prepared composites in 3 M KOH aqueous solution. The average specific capacitance of the composite was calculated according to the following equation:[37,38]

$$C_s = I\Delta t/(m\Delta V) \quad (1)$$

where C_s (F g^{-1}) is the specific capacitance, I (mA) is the charge-discharge current, Δt (s) is the discharge time, ΔV (V) represents the potential drop during discharge, and m (mg) is the mass of the active material within the electrode.

Results and discussion

Synthesis of Co_3O_4/RGO composite

In this work, we have developed a facile refluxing method combined with a thermal annealing process for preparing Co_3O_4/RGO composite. Firstly, graphite oxide was ultrasonicated in deionized water to form a homogeneous GO suspension due to the oxygen-containing functional groups on the edges of GO sheets.[39] When $Co(NO_3)_2$ $6H_2O$ was added, the positively charged Co^{2+} ions were absorbed onto the negatively charged GO sheets through the electrostatic interactions. HMTA can release hydroxyl ions gradually and uniformly in the aqueous solution at high temperature, which was extensively used in the fabrication of metals hydroxides.[40] In addition, HMTA and other ammonia-related chemicals have been demonstrated to be effective reductants for the reduction

of GO at a relatively low temperature.[41-44] Thus, when HMTA was introduced into the above solution and then refluxed at 90 ℃ for 3 h, GO was converted to RGO, meanwhile uniform $Co(OH)_2$ nanosheets (Fig. S1, see Supporting Information) were formed on RGO sheets due to the well attached Co^{2+} ions. In the following step, RGO was further thermally reduced at the temperature of 300 ℃ in air, at the same time, Co_3O_4/RGO composite with porous Co_3O_4 nanosheets attached on RGO sheets was obtained due to the thermal decomposition of $Co(OH)_2$ nanosheets.

Characterization of Co_3O_4/RGO composites

The detailed morphology, size and microstructure of the as-prepared Co_3O_4/RGO composites were investigated by TEM and high-resolution TEM (HRTEM). Fig. 1 represents the

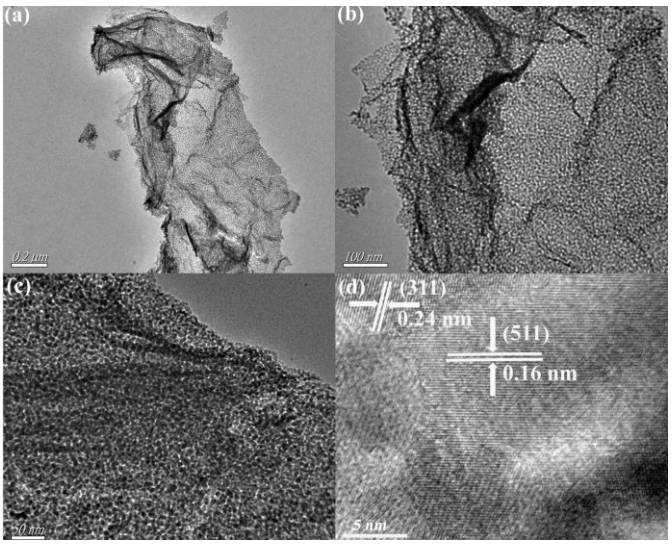

Fig. 1 (a-c) TEM images and (d) HRTEM image of Co_3O_4/RGO-0.50 composite.

typical TEM images of Co_3O_4/RGO-0.50 composite. The typical structure with rippled and crumpled feature that graphene sheets intrinsically own is observed (Fig. 1a and 1b), indicating the existence of RGO sheets in the Co_3O_4/RGO composite. The high magnification TEM image (Fig. 1c) clearly reveals the porous structure of the composite. It can be seen that the nanosheets possess numerous nanosized pores and are composed of tiny nanoparticles with a size of several nanometers. This porous structure should arise from the decomposition of cobalt hydroxide during the thermal annealing process, and such porous nanosheets are in favor of the improvement of electrochemical performance due to more active surface of the active component accessible by the electrolyte.[45] The HRTEM image (Fig. 1d) reveals two different sets of lattice fringes, in which the lattice spacings of 0.24 and 0.16 nm are attributed to the (311) and (511) planes of Co_3O_4, respectively. The SEM images of Co_3O_4/RGO-0.50 (Fig. S2, see Supporting Information) further reveal that the Co_3O_4/RGO composite possesses nanosheet structure. TEM images of other Co_3O_4/RGO composites with different loading amounts of Co_3O_4 are presented in Fig. S3 (see Supporting Information), all of these composites display the similar morphology as observed from Co_3O_4/RGO-0.50 composite. These results demonstrate that the employed synthesis strategy is highly effective for preparing Co_3O_4/RGO composites.

The TEM image of the composite sample before annealing treatment is shown in Fig. S4a (see Supporting Information), from which it can be seen that $Co(OH)_2$ nanosheets are well attached on wrinkled RGO sheets. For comparison, SEM image of the pure $Co(OH)_2$ sample before thermal treatment is provided in Fig. S4b (see Supporting Information), and the product is composed of a large number of nanosheets. The pure Co_3O_4 was further examined by (HR)TEM (Fig. 2), from which the nanosheets with porous structure are observed (Fig. 2a-2c), and the lattice fringes with the spacings of 0.24 and 0.16 nm (Fig. 2d) match well with the (311) and (511) planes of Co_3O_4, respectively. This result is well consistent with the TEM observation of CO_3O_4/RGO-0.50 composite.

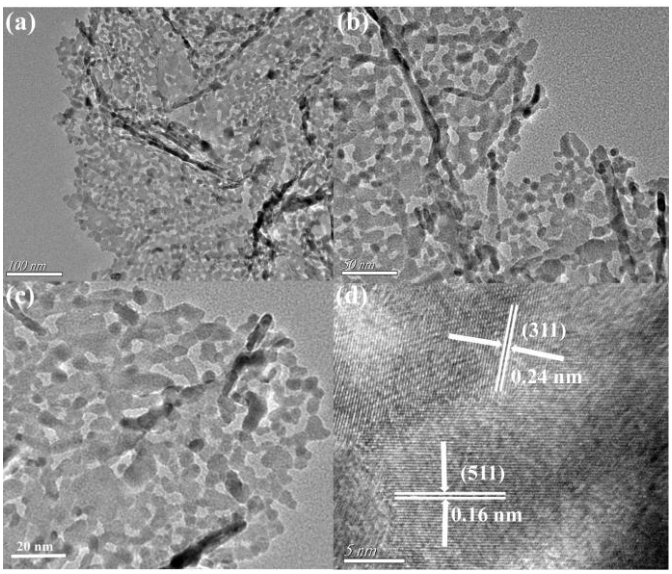

Fig. 2 (a-c) TEM images and (d) HRTEM image of Co_3O_4 nanosheets.

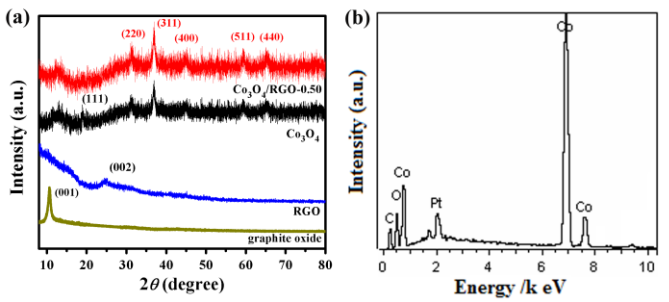

Fig. 3 (a) XRD patterns of graphite oxide, RGO, Co_3O_4 and Co_3O_4/RGO-0.50 composite; and (b) the EDS spectrum of Co_3O_4/RGO-0.50 composite.

Fig. 3a presents the XRD patterns of graphite oxide, RGO, Co_3O_4 and Co_3O_4/RGO-0.50 composite. The XRD pattern of graphite oxide shows a sharp diffraction peak centered at 2θ = 10.3 º, corresponding to the (001) peak of graphite oxide. The disappearance of the (001) peak in the XRD patterns of RGO

and Co_3O_4/RGO-0.50 composite demonstrate that graphite oxide has been well flaked to GO and/or successfully reduced into RGO during the synthesis process. In contrast, a new broad diffraction peak at 2θ = 24.9 º was observed for RGO, which can be ascribed to the (002) reflection of graphene sheets.[41] The diffraction peaks located at 2θ values of 31.3 º, 36.8 º, 44.8 º, 59.3 ºand 65.2 ºin the XRD patterns of Co_3O_4 and Co_3O_4/RGO-0.50 composite can be easily indexed to the (220), (311), (400), (511) and (440) reflections of cubic Co_3O_4 (JPCDS No.43-1003). It should be noted here that the weak and broad peak at 2θ = 13 º originates from the SiO_2 substrate used for XRD measurement.[46] The EDS spectrum of Co_3O_4/RGO-0.50 composite is presented in Fig. 3b. It demonstrates that carbon, oxygen and cobalt elements were detected from the Co_3O_4/RGO composite. The carbon element comes from the RGO sheets, while the oxygen element derives from porous Co_3O_4 nanosheets and the residual oxygen-containing groups on RGO sheets. The actual contents of Co_3O_4 in the as-prepared Co_3O_4/RGO composites were investigated by ICP-OES (Table S1, see Supporting Information). It was found that the content of Co_3O_4 increases from 75.2 to 94.4% with the increase of feeding amount of $Co(NO_3)_2$ $6H_2O$ used in the synthesis.

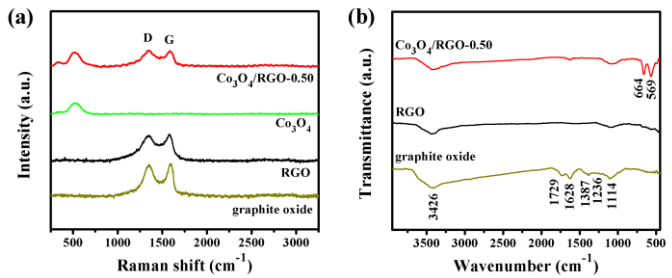

Fig. 4 (a) Raman and (b) FT-IR spectra of graphite oxide, RGO and Co_3O_4/RGO-0.50 composite. The Raman spectrum of Co_3O_4 is also shown for comparison.

Raman spectroscopy is a widely used tool for evaluating the disorder and defect structures of graphene-based materials.[47] Fig. 4a shows the Raman spectra of graphite oxide, RGO, Co_3O_4 and Co_3O_4/RGO-0.50 composite. The Raman spectra of graphite oxide, RGO and Co_3O_4/RGO-0.50 composite display two prominent peaks, corresponding to the D and G band of carbon, respectively. The D band, observed at about 1350 cm^{-1}, is associated with structural defects and disorders that break the symmetry and selection rule, while the G band, at about 1590 cm^{-1}, is usually assigned to the E_{2g} phonon of C sp^2 atoms.[48] The integrated intensity ratio of D to G band, denoted as I_D/I_G, is associated with the conjugated graphene network (sp^2 domain) of graphene sheets. The I_D/I_G values for graphite oxide, RGO and Co_3O_4/RGO-0.50 composite are *ca.* 1.91, 2.36 and 2.46, respectively. Compared with graphite oxide, the increment of I_D/I_G value for RGO suggests a decrease in the average size of the sp^2 domains, indicating that GO has been well flaked and reduced. The sp^2 domain is re-established after chemical reduction; however, the size of the re-established graphene network is usually smaller than original graphite oxide, which will consequently lead to an increase of I_D/I_G value.[49] For Co_3O_4/RGO-0.50 composite, a further increased I_D/I_G value was obtained. This result can be attributed to the attachment of Co_3O_4 nanosheets on RGO sheets, which can stress its surface and induce more defects and disorders.[50] In addition, the Raman peaks at about 520 cm^{-1} in the Raman spectra of Co_3O_4 nanosheets and Co_3O_4/RGO-0.50 composite can be attributed to the F_{2g} mode of Co_3O_4, which is well consistent with the previous reports.[51,52]

The FT-IR spectra in Fig. 4b further confirm the successful reduction of GO. The absorptions relate to oxygen-containing groups are observed in the FT-IR spectrum of graphite oxide. In detail, the absorption bands at 3426 and 1387 cm^{-1} can be assigned to the stretching vibration and deformation vibration of O-H, respectively. The band at 1729 cm^{-1} belongs to the C=O stretching vibration of COOH groups.[53] The stretching vibration peaks of C-O (epoxy) and C-O (alkoxy) are observed at 1236 and 1114 cm^{-1}, respectively. The band at 1628 cm^{-1} derives from the vibration of the adsorbed water molecules and/or the contribution of the skeletal vibration of unoxidized graphitic domains. However, in the FT-IR spectra of RGO and Co_3O_4/RGO-0.50 composite, the above absorption bands disappear or diminish greatly, indicating the successful reduction of GO.[54,55] The strong bands at 663 and 568 cm^{-1} in the FT-IR spectrum of Co_3O_4/RGO-0.50 composite can be assigned to the stretching vibration mode of Co-O bond.[56-58]

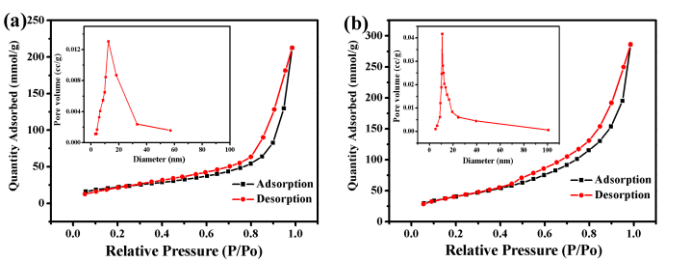

Fig. 5 Nitrogen adsorption and desorption isotherms of (a) porous Co_3O_4 sheets and (b) Co_3O_4/RGO-0.50 composite. The insets of (a) and (b) show the pore size distribution of Co_3O_4 sheets and Co_3O_4/RGO-0.50 composite, respectively.

The specific surface area of the as-prepared products was also investigated by BET technique. Fig. 5 displays the nitrogen adsorption and desorption isotherms of Co_3O_4 nanosheets and Co_3O_4/RGO-0.50 composite, the specific surface areas for Co_3O_4 nanosheets and Co_3O_4/RGO-0.50 composite are 78.4 and 152.3 m^2/g, respectively, and the pore sizes for Co_3O_4 nanosheets and Co_3O_4/RGO-0.50 composite are about 13.7 and 9.4 nm, respectively. The big specific surface area of Co_3O_4 may originate from the porous structure of the Co_3O_4 nanosheet. Such a structure is favorable for supercapacitor application because the porous structure with a large specific surface area can facilitate the electrolyte ion diffusion and provide more electroactive sites for fast energy storage.[59] The much higher specific surface area of Co_3O_4/RGO-0.50 composite compared to pure Co_3O_4 nanosheets can be ascribed to the existence of RGO sheets in Co_3O_4/RGO-0.50 composite, which effectively prevent the agglomeration of Co_3O_4 nanosheets and RGO sheets themselves. Therefore, the combination of RGO and

Co_3O_4 nanosheets can not only facilitate the penetration of electrolytes into the inner part and shorten the ionic diffusion path, but also provide a large surface area for the adsorption of ions and charge-transfer reactions.[60,61]

Electrochemical behavior

Considering the unique structural feature and the potential excellent performance, the Co_3O_4/RGO composites as electrode materials for supercapacitors were investigated by CV and charge-discharge measurements in 3 M KOH aqueous solution. Fig. 6a shows the typical CV curves of Co_3O_4/RGO composites, Co_3O_4 and RGO electrodes at a scan rate of 5 mV s^{-1}. The CV shapes clearly reveal the pseudocapacitive characteristics of the as-prepared Co_3O_4/RGO composites and Co_3O_4 nanosheets. Two pairs of redox peaks are observed in each CV curve, the reduction peak of P_1 and the corresponding oxidation peak of P_2 is related to the redox reaction: $Co_3O_4 + H_2O + OH^- = 3CoOOH + e^-$, while the reduction peak of P_3 and the corresponding oxidation peak of P_4 is associated with the following redox reaction: $CoOOH + OH^- = CoO_2 + H_2O + e^-$.[24] The specific capacitance values are calculated by the formula: $C_s = (\int I(V)dV)/(vm\Delta V)$,[62] where I is the response current, ΔV is the potential range, v is the potential scan rate, and m is the mass of the active materials used in the electrode. From the CV curves in Fig. 6a, the specific capacitance values at the scan rate of 5 mV s^{-1} were determined to be 417.6, 453.7, 428.6, 315.6, 257.4 and 52.5 F g^{-1} for Co_3O_4/RGO-0.25, Co_3O_4/RGO-0.50, Co_3O_4/RGO-0.75, Co_3O_4/RGO-1.0, Co_3O_4 and RGO, respectively. Co_3O_4/RGO-0.50 composite exhibits the highest specific capacitance value among all of these samples. Fig. 6b presents the CV curves of Co_3O_4/RGO-0.50 electrode at various scan rates of 5, 10, 20 and 40 mV s^{-1}. It can be observed that the CV curve becomes wider with the increasing scan rates from 5 to 40 mV s^{-1}, however, the specific capacitance decreases with the increase of scan rates. At a high scan rate of 40 mV s^{-1}, almost 47.9% capacitance retention is observed, much higher than that of Co_3O_4 nanosheets (28.3%, as shown in Fig. 6c), suggesting a better rate capability of Co_3O_4/RGO composite electrode.[63] In addition, according to the slopes shown in Fig. 6d, the diffusion coefficient of electrolyte ions for Co_3O_4/RGO-0.50 composite electrode is 1.98 times higher than that of Co_3O_4 nanosheets electrode, suggesting that the Co_3O_4/RGO composite electrode has better ions diffusion than pure Co_3O_4.[64]

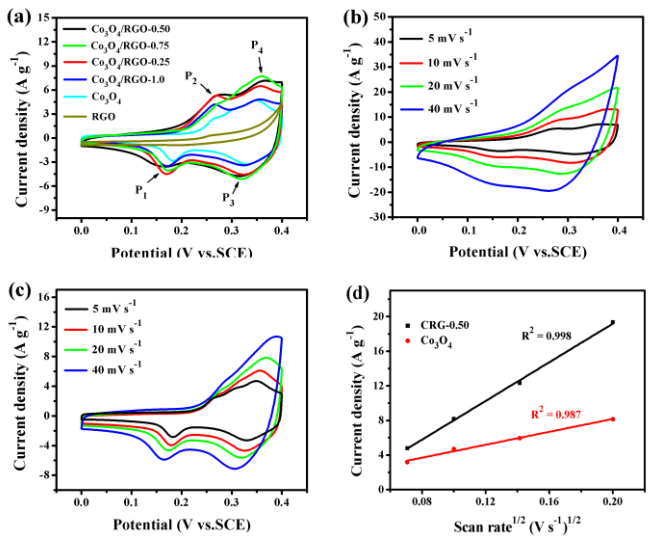

Fig. 6 (a) CV curves of Co_3O_4/RGO composites, Co_3O_4 and RGO electrodes at the scan rate of 5 mV s^{-1}. The CV curves of (b) Co_3O_4/RGO-0.50 electrode and (c) Co_3O_4 porous nanosheet electrode at various scan rates. (d) The variation of the current densities of the cathodic peaks (P_3) for Co_3O_4/RGO-0.50 composite and Co_3O_4 nanosheet electrodes as a function of the square root of scan rate.

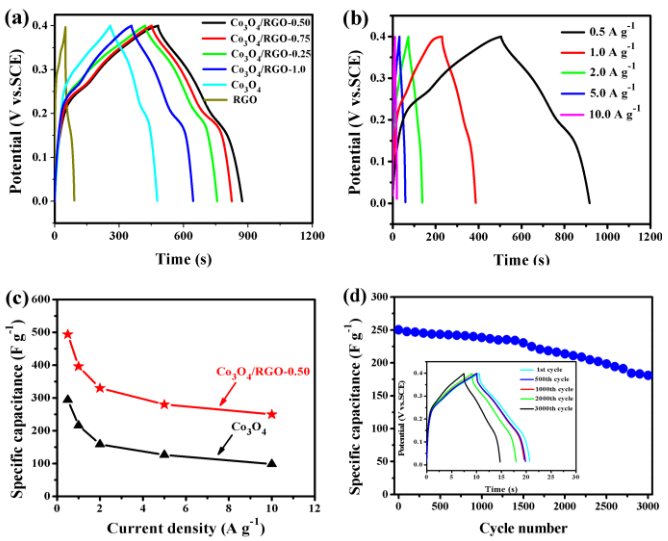

Fig. 7 (a) Charge-discharge curves of Co_3O_4/RGO composites, Co_3O_4 nanosheets and RGO electrodes at the current density of 0.5 A g^{-1}; (b) charge-discharge curves of Co_3O_4/RGO-0.50 electrode at various current densities of 0.5, 1.0, 2.0, 5.0 and 10.0 A g^{-1}; (c) the specific capacitance values of Co_3O_4/RGO-0.50 composite and Co_3O_4 electrodes as a function of current density; (d) the cycling performance of Co_3O_4/RGO-0.50 electrode at a constant current density of 10 A g^{-1}. The inset of (d) shows the charge-discharge curves of the 1st, 500th, 1000th, 2000th and 3000th cycle.

Fig. 7a displays the charge-discharge curves of the Co_3O_4/RGO composites, pure Co_3O_4 nanosheets and RGO electrodes at the current density of 0.5 A g^{-1}. The calculated specific capacitance values for Co_3O_4/RGO-0.25, Co_3O_4/RGO-0.50, Co_3O_4/RGO-0.75, Co_3O_4/RGO-1.0, Co_3O_4 nanosheets and RGO electrodes are 421.3, 518.8, 463.6, 387.4, 294.5 and 72.8 F g^{-1}, respectively. Evidently, Co_3O_4/RGO electrodes possess much higher specific capacitance values than pure Co_3O_4 and RGO electrodes. Among them, Co_3O_4/RGO-0.50 composite exhibits the highest specific capacitance, which is well consistent with the result obtained from CV curves. Because RGO exhibits a specific capacitance value as low as 72.8 F g^{-1}, the higher specific capacitance for Co_3O_4/RGO composites can be attributed to the synergistic effect between RGO support and Co_3O_4 porous nanosheets. The RGO support with large surface area allows more dispersed Co_3O_4 nanoparticles, giving better material utilization for capacitance generation. The high electrical conductivity of RGO improves the charge transfer and charge transport necessary for relevant

redox reactions. The residual oxygen-containing groups on RGO ensure good bonding, interfacial interactions and electrical contacts between RGO sheets and Co_3O_4 nanosheets.[65] In addition, the specific capacitances of the Co_3O_4/RGO composites strongly depend on the loading amount of Co_3O_4 nanosheets. The specific capacitance of Co_3O_4/RGO electrodes increase at first and then decrease with the increase of Co_3O_4 content in Co_3O_4/RGO composites. In Co_3O_4/RGO electrodes, Co_3O_4 predominates in charge storage, while RGO sheets act as electronic conductive channels. Therefore, it is reasonable that the specific capacitance increases with the increase of Co_3O_4 content within a certain range. However, as evidenced by the TEM images (Fig. 1 and Fig. S3, see Fig. S3 in Supporting Information) and XRD patterns (Fig. S5, see Supporting Information) of the Co_3O_4/RGO composites, the increase of Co_3O_4 content in the Co_3O_4/RGO composites will accordingly reduce the relative content of RGO. The Co_3O_4 nanosheets tend to aggregate together (Fig. S3c-3f, see Supporting Information) and the conductivity of the composites would decrease, thus contributing to the decrement of specific capacitance values. Therefore, a suitable content of Co_3O_4 in Co_3O_4/RGO composites is critical to optimizing the capacitance performance.

Fig. 7b presents the charge-discharge curves of Co_3O_4/RGO-0.50 electrode at various current densities. It can be observed that the discharge time decreases with the increase of current density from 0.5 to 10 A g^{-1}. The specific capacitance of the electrode was calculated according to equation (1). The specific capacitance values for Co_3O_4/RGO-0.50 electrode at the current density of 0.5, 1.0, 2.0, 5.0 and 10.0 A g^{-1} are 518.8, 396.4, 330.2, 280.6 and 246.7 F g^{-1}, respectively. The calculated specific capacitance values of Co_3O_4/RGO-0.50 and Co_3O_4 electrodes as a function of current density are shown in Fig. 7c, from which it can be concluded that the rate capability of Co_3O_4/RGO-0.50 composite electrode (47.5%) is better than that of Co_3O_4 electrode (32.5%), which is well consistent with the result obtained from CV curves.

Electrochemical stability is another important factor for evaluating electrode materials.[66] The cycling stability of Co_3O_4/RGO-0.5 electrode was evaluated by repeating the charge-discharge measurements at a constant current density of 10 A g^{-1}. Fig. 7d shows specific capacitance values of the initial 3000 cycles as a function of cycle number, and the inset displays the charge-discharge curves of the 1st, 500th, 1000th, 2000th and 3000th cycle. The specific capacitance values remain almost constant in the first 1500 cycles with a small capacitance loss of 7.6%, and then decrease gradually in the residual cycles with a decay of 27.7% at the end of the 3000th cycle.

Compared with the reported Co_3O_4/RGO composites,[28-32] our Co_3O_4/RGO composite possesses better capacitive performance. For instances, Zhang *et al.* synthesized Co_3O_4/RGO composite with Co_3O_4 hollow spheres deposited on RGO sheets, which delivers a specific capacitance of 340 F g^{-1} at the current density of 1.0 A g^{-1}.[29] Guan *et al.* prepared a composite with the needle-like Co_3O_4 deposited on RGO sheets, the composite as electrode material exhibits a specific capacitance of 81.7 F g^{-1} at the current density of 0.5 A g^{-1}.[31] A maximum specific capacitance of 445.0 F g^{-1} at the current density of 0.5 A g^{-1} was obtained with the Co_3O_4 nanoparticles/RGO composite as the electrode materials.[28,30,32] In this study, our Co_3O_4/RGO composite exhibits a specific capacitance of 518.8 F g^{-1} at the current density of 0.5 A g^{-1}, much higher than those of reported. This result can be attributed to the unique microstructure of our Co_3O_4/RGO composites. The attachment of porous Co_3O_4 nanosheets on RGO sheets can form a perfect integrated structure with developed electron conductive networks and shortened ion transport paths, ensuring the maximum utilization of the combined advantages of both RGO and Co_3O_4. In addition, although our Co_3O_4/RGO composites show a little lower specific capacitance than some other Co_3O_4 based electrode materials, such as $Co_3O_4/RuO_2 \cdot xH_2O$ composite (642 F g^{-1} at 1.0 A g^{-1})[67] and Co_3O_4/SiO_2 composite (679 F g^{-1} at 1.0 A g^{-1})[68], the cost of our Co_3O_4/RGO composites is relatively lower and the synthesis method is simple and facile, which provide a main technique advantage over those reported composites. This result further demonstrates that our Co_3O_4/RGO composites are the promising electrode materials for practical applications.

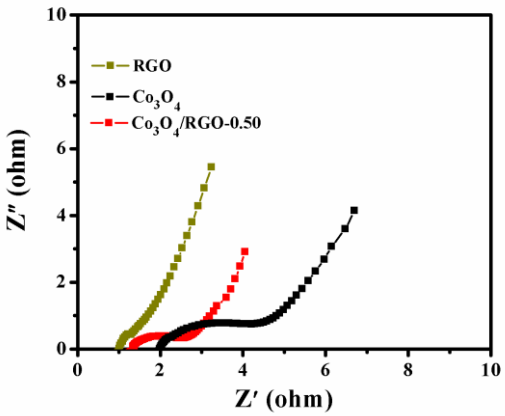

Fig. 8 EIS of Co_3O_4/RGO-0.50, Co_3O_4 and RGO electrodes.

The EIS measurements for the Co_3O_4/RGO, Co_3O_4 and RGO electrodes were conducted in 3 M KOH solution, and the results are provided in Fig. 8. All the plots show a similar shape, which consists of a semicircle in the high frequency region and a straight line in the low frequency region. The charge transfer resistance (R_{ct}) in the high frequency region corresponded to the diameter of a semicircle. It can be observed from Fig. 8 that the RGO electrode possesses the smallest diameter, and Co_3O_4/RGO-0.50 electrode exhibits a smaller diameter than pure Co_3O_4 electrode, suggesting that Co_3O_4/RGO-0.50 electrode possesses smaller R_{ct} value. This result indicates that the electrochemical reaction on the electrode/electrolyte interface for Co_3O_4/RGO electrode is more facile than pure Co_3O_4 electrode. Meanwhile, the value of the intercept at the real axis in the high frequency region can be used to estimate

the resistance arising from the electrolyte (R_Ω). It can be observed that the Co_3O_4/RGO-0.50 electrode shows smaller R_Ω value than pure Co_3O_4, but higher than that of RGO. These results demonstrate that the incorporation of RGO could significantly improve the electrical performance of Co_3O_4/RGO electrodes.[31,69]

Conclusions

In summary, Co_3O_4/RGO composites with porous Co_3O_4 nanosheets attached on RGO sheets are synthesized through a facile refluxing procedure followed by a thermal annealing process. The Co_3O_4/RGO composites exhibit a high specific capacitance up to 518.8 F g^{-1} at the current density of 0.5 A g^{-1}, and great cycle stability with a decay of about 7.6% after 1500 cycles at the high current density of 10 A g^{-1}. The excellent capacitive performance of the Co_3O_4/RGO composites can be mainly attributed to the porous nanosheet structure of Co_3O_4 as well as its effective combination with RGO. RGO not only acts as an ideal substrate for uniformly anchoring of Co_3O_4 nanosheets, but also serves as conductivity additive for improving the conductivity and ions transfer pathways of Co_3O_4/RGO composites. This approach offers a facile strategy to synthesize graphene-metal oxide electrode materials with porous structure. The remarkable capacitive performance of the Co_3O_4/RGO composites demonstrates their potential application in electrode materials for supercapacitors.

Acknowledgements

The authors are grateful for financial support from National Nature Science Foundation of China (No. 51272094), Specialized Research Fund for the Doctoral Program of Higher Education of China (No. 20123227110018), China Postdoctoral Science Foundation (2014M561578) and Jiangsu Planned Projects for Postdoctoral Research Funds (1401109C).

Notes and references

[a] School of Chemistry and Chemical Engineering, Jiangsu University, Zhenjiang 212013, P. R. China, Fax: (+86)511-88791800; Tel: (+86)511-88791800; E-mail: xiaopingshen@163.com

[b] School of Material Science and Engineering, Jiangsu University, Zhenjiang 212003, P. R. China

[c] School of Material Science and Engineering, Jiangsu University of Science and Technology, Zhenjiang 212003, P. R. China

1 Y. Huang, X. L. Huang, J. S. Lian, D. Xu, L. M. Wang and X. B. Zhang, *J. Mater. Chem.*, 2012**,** **22**, 2844-2847.

2 M. Zhang and M. Q. Jia, *J. Alloys Compd.*, 2013**,** **551**, 53-60.

3 R. Kotz and M. Carlen, *Electrochim. Acta*, 2000, **45**, 2483-2498.

4 P. H. Yang, X. Xiao, Y. Z. Li, Y. Ding, P. F. Qiang, X. H. Tan, W. J. Mai, Z. Y. Lin, W. Z. Wu, T. Q. Li, H. Y. Jin, P. Y. Liu, J. Zhou, C. P. Wong and Z. L. Wang, *ACS Nano*, 2013, **7**, 2617-2626.

5 H. L. Wang, Q. L. Hao, X. J. Yang and L. D. Lu, *Electrochem. Commun.*, 2009, **11**, 1158-1161.

6 L. Yu, G. Q. Zhang, C. Z. Yuan and X. W. Lou, *Chem. Commun.*, 2013, **49**, 137-139.

7 C. C. Hu, K. H. Chang, M. C. Lin and Y. T. Wu, *Nano Lett.*, 2006, **6**, 2690-2695.

8 Z. Y. Lu, Q. Yang, W. Zhu, Z. Chang, J. F. Liu, X. M. Sun, D. G. Evans and X. Duan, *Nano Res.*, 2012, **5**, 369-378.

9 Y. U. Jeong and A. Manthiram, *J. Electrochem. Soc.*, 2002, **149**, A1419-A1422.

10 T. Zhu, Z. Wang, S. Ding, J. S. Chen and X. W. Lou, *RSC Adv.*, 2011, **1**, 397-400.

11 J. Yang, X. Duan, Q. Qin and W. Zheng, *J. Mater. Chem. A*, 2013, **1**, 7880-7884.

12 S. W. Chou and J. Y. Lin, *J. Electrochem. Soc.*, 2013, **160**, D178-D182.

13 H. Zhang, X. Yu, D. Guo, B. Qu, M. Zhang, Q. Li and T. Wang, *ACS Appl. Mater. Interfaces*, 2013, **5**, 7335-7340.

14 Z. Xing, Q. Chu, X. Ren, J. Tian, A. M. Asiri, K. A. Alamry, A. O. Al-Youbi and X. Sun, *Electrochem. Commun.*, 2013, **32**, 9-13.

15 Y. Liu, H. W. Huang and X. S. Peng, *Electrochim. Acta*, 2013, **104**, 289-294.

16 S. J. He and W. Chen, *J. Power sources*, 2014, **262**, 391-400.

17 S. Guo and S. Dong, *Chem. Soc. Rev.*, 2011, **40**, 2644-2672.

18 A. K. Geim and K. S. Novoselov, *Nat. Mater.*, 2007, **6**, 183-191.

19 Y. Liu, D. Yan, R. F. Zhuo, S. K. Li, Z. G. Wu, J. Wang, P. Y. Ren, P. X. Yan and Z. R. Geng, *J. Power Sources*, 2013, **242**, 78-85.

20 S. M. Paek, E. Yoo and I. Honma, *Nano Lett.*, 2009, **9**, 72-75

21 Z. S. Wu, D. W. Wang, W. Ren, J. Zhao, G. Zhou, F. Li and H. M. Cheng, *Adv. Funct. Mater.*, 2010, **20**, 3595-3602.

22 G. Wang, J. Bai, Y. Wang, Z. Ren and J. Bai, *Scr. Mater.*, 2011, **65**, 339-342.

23 J. Hu, A. Ramadan, F. Luo, B. Qi, X. Deng and J. Chen, *J. Mater. Chem.*, 2011, **21**, 15009-15014.

24 C. Xu, X. Wang, L. C. Yang and Y. P. Wu, *J. Solid State Chem.*, 2009, **182**, 2486-2490.

25 J. H. Pan, Q. Z. Huang, Z. Y. Koh, D. Neo, X. Z. Wang and Q. Wang, *ACS Appl. Mater. Interfaces*, 2013, **5**, 6292-6299.

26 S. K. Meher, P. Justin and G. R. Rao, *ACS Appl. Mater. Interfaces*, 2011, **3**, 2063-2073.

27 M. J. Deng, F. L. Huang, I. W. Sun, W. T. Tsai and J. K. Chang, *Nanotechnology*, 2009, **20**, 175602.

28 G. J. Liu, L. Q. Fan, F. D. Yu, J. H. Wu, L. Liu, Z. Y. Qiu and Q. Liu. *J. Mater. Sci.*, 2013, **48**, 8463-8470.

29 D. H. Zhang and W. B. Zou, *Current Applied Physics* 2013, **13**, 1796-1800.

30 X. D. Huang, B. Sun, S. Q. Chen and G. X. Wang. *Chem. Asian J.*, 2014, **9**, 206-211.

31 Q. Guan, J. L. Cheng, B. Wang, W. Ni, G. F. Gu, X. D. Li, L. Huang, G. C. Yang and F. D. Nie, *ACS Appl. Mater. Interfaces*, 2014, **6**, 7626-7632.

32 S. Park and S. Kim, *Electrochim. Acta*, 2013, **89**, 516-522.

33 Y. B. Zhang and Z. G. Guo, *Chem. Commun.*, 2014, **50**, 3443-3446.

34 C. Yuan, J. Li, L. Hou, X. Zhang, L. Shen and X. W. Lou, *Adv. Funct. Mater.*, 2012, **22**, 4592-4597.

35 F. Z. Deng, L. Yu, G. Cheng T. Lin, M. Sun, F. Ye and Y. F. Li, *J. Power Sources*, 2014, **251**, 202-207.

36 Z. Y. Ji, X. P. Shen, J. L. Yang, G. X. Zhu and K. M. Chen, *Appl. Catal. B*, 2014, **144**, 454-461.

37 Z. J. Luo, K. Wang, H. M. Li, S. Yin, Q. F. Guan and L. G. Wang, *CrystEngComm*., 2011, **13**, 7108-7113.
38 H. Chen, L. F. Hu, M. Chen, Y. Yan and L. M. Wu, *Adv. Funct. Mater*., 2014, **24**, 934-942.
39 Z. Y. Ji, G. X. Zhu, X. P. Shen, H. Zhou, C. M. Wu and M. Wang, *New J. Chem*., 2012, **36**, 1774-80..
40 G. Q. Zhang and X. W. Lou, *Sci. Rep.*, 2013, **3**, 1470.
41 X. P. Shen, L. Jiang, Z. Y. Ji, J. L. Wu, H. Zhou and G. X. Zhu, *J. Collid Interface Sci*., 2011, **354**, 493-497.
42 X. S. Du, C. F. Zhou, H. Y. Liu, Y. W. Mai and G. X. Wang, *J. Power Sources*, 2013, **24**, 460-466.
43 J. J. Lin, T. Mei, M. J. Lv, C. A. Zhang, Z. F. Zhao and X. B. Wang, *RSC Adv.*, 2014, **4**, 29563-29570.
44 G. Q. Tang, Z. G. Jiang, X. F. Li, H. B. Zhang, A. Dasari and Z. Z. Yu, *Carbon*, 2014, **77**, 592-599.
45 F. Y. Cheng, J. Z. Zhao, W. N. Song, C. S. Li, H. Ma, J. Chen and P. W. Shen, *Inorg. Chem*., 2006, **45**, 2038-2044.
46 Z. Y. Ji, X. P. Shen, J. L. Yang, Y. L. Xu, G. X. Zhu and K. M. Chen, *Eur. J. Inorg. Chem.*, 2013, **2013**, 6119-6125.
47 S. Bi, T. T. Zhao, X. Q. Jia and P. He, *Biosens. Bioelectron*., 2014, **57**, 110-116.
48 N. N. Hong, L. Song, B. B. Wang, B. B. Yuan, Y. Q. Shi and Y. Hu, *J. Appl. Polym. Sci.*, 2014, **131**, 40457.
49 M. A. Pimenta, G. Dresselhaus, M. S. Dresselhaus, L. G. Cancado, A. Jorio and R. Saito, *Phys. Chem. Chem. Phys.*, 2007, **9**, 1276-1290.
50 Y. Y. Wen, H. M. Ding and Y. K. Shan, *Nanoscale*, 2011, **3**, 4411-4417.
51 J. H. Jiang, W. D. Shi, S. Y. Song, Q. L. Hao, W. Q. Fan, X. F. Xia, X. Zhang, Q. Wang, C. B. Liu and D. Yan, *J. Power. Sources*, 2014, **248**, 1281-1289.
52 P. B. Liu, Y. Huang and X. Sun, *ACS Appl. Mater. Interfaces*, 2013, **5**, 12355-12360.
53 Z. Y. Huang, H. H. Zhou, C. H. Li, F. Y. Zeng, C. P. Fu and Y. F. Kuang, *J. Mater. Chem.*, 2012, **22**, 1781-1785.
54 L. Ye, J. L. Fu, Z. Xu, R. S. Yuan and Z. H. Li, *ACS Appl. Mater. Interfaces*, 2014, **6**, 3483-3490.
55 S. Park, J. H. An, I. W. Jung, R. D. Piner, D. Richard, S. J. An, X. S. Li, A. Velamakanni and R. S. Ruoff, *Nano Lett.*, 2009, **9**, 1593-1597.
56 Z. Z. Zhu, G. Z. Lu, Z. G. Zhang, Y. Guo, Y. L. Guo and Y. Q. Wang, *ACS Catal*., 2013, **3**, 1154-1164.
57 H. S. Soo, A. Agiral, A. Bachmeier and H. Frei, *J. Am. Chem. Soc*., 2012, **134**, 17104-17116.
58 P. H. Shi, R. J. Su, F. Z. Wan, M. C. Zhu, D. X. Li and S. H. Xu, *Appl. Catal. B*, 2012, **123**, 265-272.
59 J. Zhang, L. B. Kong, J. J. Cai, H. Li, Y. C. Luo and L. Kang, *Microporous Mesoporous Mater*., 2010, **132**, 154-162.
60 X. Y. Yu, X. Z. Yao, T. Luo, Y. Jia, J. H. Liu and X. J. Huang, *ACS Appl. Mater. Interfaces*, 2014, **6**, 3689-3695.
61 J. Pu, J. Wang, X. Q. Jin, F. L. Cui, E. H. Sheng and Z. H. Wang, *Electrochim. Acta*, 2013, **106**, 226-234.
62 G. N. Zhang, L. Zheng, M. Zhang, S. H. Guo, Z. H. Liu, Z. P. Yang and Z. L. Wang, *Energy Fuels*, 2012, **26**, 618-623.
63 L. J. Deng, Z. P. Hao, J. F. Wang, G. Zhu, L. P. Kang, Z. H. Liu, Z. P. Yang and Z. L. Wang, *Electrochim. Acta*, 2013, **89**, 191-198.
64 C. S. Dai, P. Y. Chien, J. Y. Lin, S. W. Wei, W. K. Wu, P. H. Li, K. Y. Wu and T. W. Lin, *ACS Appl. Mater. Interfaces*, 2013, **5**, 12168-12174.
65 Z. S. Wu, G. M. Zhou, L. C. Yin, W. C. Ren, F. Li and H. M. Cheng, *Nano Energy*, 2012, **1**, 107-131.
66 S. Z. Li, J. Wen, X. M. Mo, H. Long, H. N. Wang, J. B. Wang and G. J. Fang, *J. Power Sources*, 2014, **256**, 206-211.
67 Y. Liu, W. W. Zhao and X. G. Zhang, *Electrochim. Acta*, 2008, **53**, 3296-3304.
68 G. A. M. Ali, O. A. Fouad, S. A. Makhlouf, M. M. Yusoff and K. F. Chong, *J. Solid State Electrochem.*, 2014, **18**, 2505-2512.
69 S. Huang, Y. H. Jin and M. Q. Jia, *Electrochim. Acta*, 2013, **95**, 139-145.

Table of Contents Entry

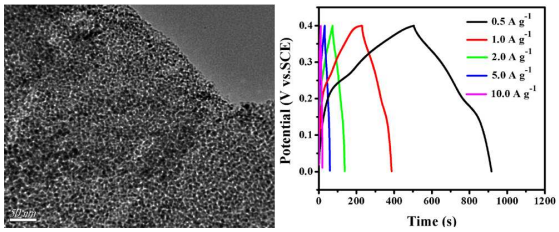

Porous Co_3O_4 nanosheets/RGO composite with excellent capacitive performance was prepared through a facile two-step strategy.